

Numerical Modeling of Pore Pressure Influence on Fracture Evolution in Brittle Heterogeneous Rocks

S. Y. Wang · S. W. Sloan · S. G. Fityus ·
D. V. Griffiths · C. A. Tang

Received: 28 March 2012 / Accepted: 27 October 2012 / Published online: 15 November 2012
© Springer-Verlag Wien 2012

Abstract Rock is a heterogeneous geological material. When rock is subjected to internal hydraulic pressure and external mechanical loading, the fluid flow properties will be altered by closing, opening, or other interaction of pre-existing weaknesses or by induced new fractures. Meanwhile, the pore pressure can influence the fracture behavior on both a local and global scale. A finite element model that can consider the coupled effects of seepage, damage and stress field in heterogeneous rock is described. First, two series of numerical tests in relatively homogeneous and heterogeneous rocks were performed to investigate the influence of pore pressure magnitude and gradient on initiation and propagation of tensile fractures. Second, to examine the initiation of hydraulic fractures and their subsequent propagation, a series of numerical simulations of the behavior of two injection holes inside a saturated rock mass are carried out. The rock is subjected to different

initial in situ stress ratios and to an internal injection (pore) pressure at the two injection holes. Numerically, simulated results indicate that tensile fracture is strongly influenced by both pore pressure magnitude and pore pressure gradient. In addition, the heterogeneity of rock, the initial in situ stress ratio (K), the distance between two injection holes, and the difference of the pore pressure in the two injection holes all play important roles in the initiation and propagation of hydraulic fractures. At relatively close spacing and when the two principal stresses are of similar magnitude, the proximity of adjacent injection holes can cause fracturing to occur in a direction perpendicular to the maximum principal stress.

Keywords Pore pressure magnitude · Pore pressure gradient · Heterogeneity · Hydraulic fractures · Numerical simulation

S. Y. Wang (✉) · S. W. Sloan · S. G. Fityus
ARC Centre of Excellence for Geotechnical Science
and Engineering, The University of Newcastle,
Callaghan, NSW 2308, Australia
e-mail: Shanyong.Wang@newcastle.edu.au

S. W. Sloan
e-mail: Scott.Sloan@newcastle.edu.au

S. G. Fityus
e-mail: Stephen.Fityus@newcastle.edu.au

D. V. Griffiths
Department of Civil and Environmental Engineering,
Colorado School of Mines, Golden, CO 80401, USA
e-mail: vgriffit@mines.edu

C. A. Tang
School of Civil and Hydraulic Engineering, Dalian University
of Technology, Dalian 116024, People's Republic of China
e-mail: catang@mechsoft.cn

1 Introduction

Hydraulic fracturing is a common technique that has been used in petroleum engineering, the mining industry, and geotechnical engineering for many years. Over the past four decades, many researchers have studied hydraulic fracturing behavior (Hubbert and Willis 1957; Haimson and Fairhurst 1969; Bjerrum et al. 1972; Medlin and Masse 1979; Rubin 1983; Lo and Kaniaru 1990; Guo et al. 1993; Yanagisawa and Panah 1994; Detournay and Cheng 1998; Detournay et al. 1989; Detournay and Atkinson 2000; Hossain et al. 2000; Crosby et al. 2002; Bohloli and de Pater 2006; Boutt et al. 2009). In general, hydraulic fractures are created in the vicinity of a borehole when the effective circumferential stress at the borehole exceeds the material tensile strength (Hubbert and Willis 1957). As for

the propagation of hydraulic fracture, it is controlled by the both the internal pore pressure and applied in situ stress ratio within non-uniform pore pressure fields (Wang et al. 2009). The propagated hydraulic fractures are usually parallel to the maximum compressive far-field stress (Haimson and Fairhurst 1969).

As pointed out by Geertsma (1985) and Detournay et al. (1986), the pore pressure effects must be considered on both a local and global scale. A local increase in pore pressure magnitude around the crack tip may enhance fracture extension. However, a global increase in pore pressure magnitude may inhibit fracture by increasing the compressive in situ stresses for the field, especially for the tensile fractures. Moreover, Bruno and Nakagawa (1991) carried out experimental tests to investigate the influence of pore pressure on tensile fracture initiation and propagation direction. The experimental test results showed that the tensile fracture is influenced by both pore pressure magnitude on a local scale around the crack tip and the orientation and distribution of pore pressure gradients on a global scale.

As discussed by Berchenko and Detournay (1997), fracture deviation is controlled by two parameters: one contrasts the far-field (applied) stress deviator to a characteristic poroelastic stress; the other contrasts the stress perturbation created by the crack (which is proportional to the fracture toughness) to the characteristic poroelastic stress. If the second parameter is small enough, the fracture path can be completely predicted from the stress trajectories, prior to fracture propagation. In addition, there are several different modes of failure when rock is subjected to internal hydraulic pressure and external loading. This is because the natural tendency of rock to fail in tension due to internal hydraulic pressure is suppressed in favor of shear failure, which is a function of external stress level. Therefore, both the internal hydraulic pressure and the in situ stresses are important experimental parameters to determine the initiation and propagation of hydraulic fractures. Furthermore, it is highly likely that multiple fractures will initiate from fractured horizontal wells (Warpinski and Teufel 1987), as the initiation and propagation of fractures from the neighboring wells will influence each other. It follows that the distance between neighboring wells is another important experimental parameter. Moreover, the presence of rock mass heterogeneities such as natural fractures, joints and bedding planes are also considered important sources of multiple fractures, and so the heterogeneity of rock is also an important experimental parameter.

In addition, fluid-saturated rock failure may be studied by two different approaches (Bruno and Nakagawa 1991). The first is based on linear elastic fracture mechanics which has several attractive features, including the Griffith

assumption of critical strain energy release rate (Griffith 1920). Several researchers have applied this approach to hydraulic fracture problems (Abou-Sayed et al. 1978; Rummel 1987; Detournay et al. 1989; Bruno and Nakagawa 1991). Their investigations considered the effects of internal crack fluid pressure on the crack tip stress intensity factor, and the contribution of pore pressure to the change in total potential energy necessary for fracture extension (Bruno and Nakagawa 1991). An alternative approach to rock failure is the material strength approach, in which stress state is determined from elasticity equations, and failure is assumed to occur when the conventional effective stress exceeds the strength of the material (Jaeger 1963; Boone et al. 1986; Wang and Nakagawa 1991; Tang 1997; Tang et al. 2002). This approach allows one to obtain the load level and the location in a structure where the material first reaches failure. This point is assumed to be the location of initial cracking or crack propagation.

Although both the fracture mechanics and material strength approaches provide a general understanding of hydraulic fracturing, analytical solutions are available for just a few simplified situations with the assumption of homogeneity (Jaeger and Cook 1979; Bruno and Nakagawa 1991; Wang and Nakagawa 1991). In addition, for laboratory tests, it is not easy to quantitatively control the process of hydraulic fracture initiation and propagation, and it is difficult to measure the change of the pore pressure gradient field, due to fracture evolution in heterogeneous rock (Bruno and Nakagawa 1991). For more complicated problems, numerical modeling techniques provide a feasible alternative solution (Boutt et al. 2009). In this paper, a numerical model that can consider the coupling effect of seepage, damage and stress fields is introduced in a code called rock failure process analysis (RFPA2D) (Tang 1997). First, two series of numerical tests in relatively homogeneous and heterogeneous rocks were performed to investigate the influence of pore pressure magnitude and gradient on initiation and propagation of tensile fractures. The numerically simulated results are compared with and validated by the associated experimental results (Bruno and Nakagawa 1991). Second, another five series of numerical tests are carried out to investigate the effect of heterogeneity of rock, the initial in situ stress ratio (K), the distance between two injection holes, and the difference between the pore pressures at the two injection holes on the initiation and propagation of hydraulic fractures.

2 Brief Description of Numerical Model

The model, developed by Tang et al. (2002), is a numerical simulation tool using finite element analyses to handle progressive failure of heterogeneous, permeable rock.

In this model, the coupled effects of flow, stresses and damage (FSD) on the extension of existing/new fractures as well as the permeability of the rocks were addressed. Coupled flow and stress variations in saturated rock masses are accounted for in the program using Biot’s theory of consolidation (Biot 1941). Having included stress effects on permeability, the basic formulations of the analysis are

$$\text{Equilibrium equation: } \frac{\partial \sigma_{ij}}{\partial x_{ij}} + \rho X_j = 0 \quad (i, j = 1, 2, 3) \tag{1}$$

$$\text{Strain-displacement equation: } \varepsilon_{ij} = \frac{1}{2}(u_{i,j} + u_{j,i})$$

$$\varepsilon_v = \varepsilon_{11} + \varepsilon_{22} + \varepsilon_{33} \tag{2}$$

$$\text{Constitutive equation: } \sigma'_{ij} = \sigma_{ij} - \alpha p \delta_{ij} = \lambda \delta_{ij} \varepsilon_v + 2G \varepsilon_{ij} \tag{3}$$

$$\text{Seepage equation: } k \nabla^2 p = \frac{1}{Q} \frac{\partial p}{\partial t} - \alpha \frac{\partial \varepsilon_v}{\partial t} \tag{4}$$

$$\text{Coupling equation: } k(\sigma, p) = \zeta k_o e^{-\beta(\frac{\sigma}{3} - \alpha p)} \tag{5}$$

where σ = stress; ρ = density; X is component of body force; u = displacement; ε = strain; α = coefficient of pore water pressure; p = pore water pressure; λ = Lamé coefficient; δ = Kronecker constant; G = shear modulus; Q = Biot’s constant; k = coefficient of permeability; k_o = initial coefficient of permeability; β = a coupling parameter that reflects the influence of stress on the coefficient of permeability; and ζ (>1) = a mutation coefficient of permeability to account for the increase in permeability of the material during fracture formation. Equations (1)–(4) are derived from Biot’s theory of consolidation. Equation (5) is introduced to describe the dependency of permeability on stress and damage, and according to a negative exponential relationship.

Both tensile and shear failure modes are considered in the analysis. An element is considered to have failed in the tension mode when its minor principal stress exceeds the tensile strength of the element, as described by Eq. (6), and to have failed in the shear mode when the compressive or shear stress has satisfied the Mohr–Coulomb failure criterion given by Eq. (7) (Tang et al. 2002; Wang et al. 2009):

$$\sigma'_3 \leq -f'_t \tag{6}$$

$$F = \sigma'_1 - \sigma'_3 \frac{1 + \sin \phi'}{1 - \sin \phi'} \geq f'_c \tag{7}$$

where σ'_1 is the major effective principal stress, σ'_3 is the minor effective principal stress, ϕ' is the effective angle of friction, f'_t is the tensile failure strength of the element, and f'_c is the compressive failure strength of the element.

For an individual element, when the particular stress in the element reaches a specified strength criterion, the element begins to damage. According to isotropic elastic damage theory, the elastic modulus of element may degrade gradually as damage progresses, defined as follows (Krajcinovic 1996; Tang et al. 2002; Wang et al. 2009):

$$E = (1 - D)E_o \tag{8}$$

where D is the damage variable, and E and E_o are elastic modulus values of the damaged and the undamaged material, respectively. When the tensile stress at a Gauss point satisfies the failure criterion of Eq. (6) the damage variable is described by (Tang et al. 2002; Wang et al. 2009)

$$D = \begin{cases} 0 & \bar{\varepsilon} < \varepsilon_{to} \\ 1 - \frac{f'_{tr}}{E_o \bar{\varepsilon}} & \varepsilon_{to} \leq \bar{\varepsilon} \leq \varepsilon_{tu} \\ 1 & \bar{\varepsilon} > \varepsilon_{tu} \end{cases} \tag{9}$$

where f'_{tr} is the residual tensile strength of the element, and $\bar{\varepsilon}$ is equivalent principal strain of the element, ε_{to} is the strain at the elastic limit, or threshold strain, and ε_{tu} is the ultimate tensile strain of the element at which the element would be completely damaged. The equivalent principal strain $\bar{\varepsilon}$ is defined as (Zhu and Tang 2004)

$$\bar{\varepsilon} = \sqrt{\langle \varepsilon_1 \rangle^2 + \langle \varepsilon_2 \rangle^2 + \langle \varepsilon_3 \rangle^2} \tag{10}$$

where ε_1 , ε_2 and ε_3 are three principal strains and $\langle \rangle$ is a function defined as follows:

$$\langle x \rangle = \begin{cases} x & x \geq 0 \\ 0 & x < 0 \end{cases} \tag{11}$$

In this case, the effect on permeability can be described by (Tang et al. 2002)

$$k = \begin{cases} k_o e^{-\beta(\sigma'_3 - \alpha p)} & D = 0 \\ \zeta k_o e^{-\beta(\sigma'_3 - \alpha p)} & 0 < D \leq 1 \end{cases} \tag{12}$$

where ζ ($\zeta > 1$) is the mutation coefficient of permeability, which reflects the damage-induced permeability increase (Tang et al. 2002). The value of ζ can be obtained from experimental tests (Thallak et al. 1991; Noghabai 1999).

When the stress in an element reaches the shear strength failure criterion of Eq. (7) the damage variable is described as (Tang et al. 2002; Wang et al. 2009)

$$D = \begin{cases} 0 & \bar{\varepsilon} < \varepsilon_{cu} \\ 1 - \frac{f'_{cr}}{E_o \bar{\varepsilon}} & \varepsilon_{cu} \leq \bar{\varepsilon} \end{cases} \tag{13}$$

where f'_{cr} is the residual compressive strength, ε_{cu} is the ultimate compressive strain of the element at which the element would be completely damaged (Tang et al. 2002).

The effect on the permeability in this case can be described by (Tang et al. 2002)

$$k = \begin{cases} k_o e^{-\beta(\sigma'_1 - \alpha p)} & D = 0 \\ \xi k_o e^{-\beta(\sigma'_1 - \alpha p)} & D > 0 \end{cases} \quad (14)$$

According to Detournay et al. (1989), pore pressure influences the direction of crack propagation only via poroelastic coupling. In other words, the stress field is influenced by the pore pressure field which in turn affects the crack path. This point is the same with the theory in the current paper. The coupling stress field and hydraulics are based on Biot theory. The permeability varies as functions of the stress states in elastic deformation, and dramatically increases when the element fails (Tang et al. 2002). Both tensile and shear failure modes are controlled by the stress field according to a certain strength criterion of material.

In RFPA2D, the specified displacement (or load) is applied to the specimen incrementally in a quasi-static manner. Coupled seepage and stress analyses are performed. At each loading increment, the seepage and stress equations of the elements are solved and a coupling analysis is performed. The stress conditions of each element are then examined for failure before the next load increment is applied. If some elements are damaged in a particular step, their reduced elastic modulus and increased permeability at each stress or strain level is calculated using the above damage variable D as well as Eq. (8). Then the calculation is restarted under the current boundary and loading conditions to redistribute the stresses in the specimen until no new damage occurs. Finally, the external load (or displacement) is increased and is used as input for the next step of the analysis. Therefore, the progressive failure process of a brittle material subjected to gradually increasing static loading can be simulated. A user-friendly

pre- and post-processor is integrated in RFPA2D to prepare the input data and display the numerical results.

The heterogeneity of rock is accounted for by randomly assigning different material properties to the different elements throughout the domain of the analysis, following a Weibull distribution (Weibull 1951).

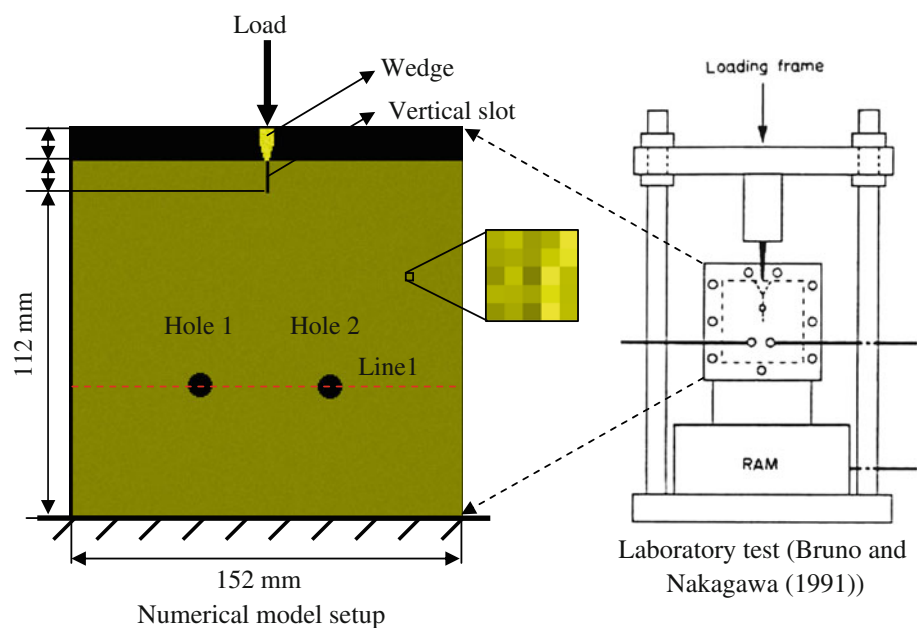
$$\varphi = \frac{m}{\mu_0} \left(\frac{\mu}{\mu_0} \right)^{m-1} \exp \left[- \left(\frac{\mu}{\mu_0} \right)^m \right] \quad (15)$$

where φ = the probability that a material property variable [such as Young's modulus (E), compressive strength (f_c) or coefficient of permeability (k)] will take on the value μ ; μ_0 = the mean value of the corresponding random variable; and m = a homogeneity index, i.e., a parameter defining the shape of the distribution function that defines the degree of material heterogeneity: a larger m implies a more homogeneous material, and vice versa.

3 Numerical Model Setup

In this paper, two kinds of numerical models were set up. The first kind was performed to investigate the influence of internal pore pressure magnitude and gradient on the propagation of tensile fractures. The numerically simulated results were compared with experimental results (Bruno and Nakagawa 1991). In these laboratory experiments, square slabs of Colton sandstone with 152 mm on a side were prepared (see Fig. 1). The permeability is about 0.04 mDa, which means the low-permeability sample. Fluid is injected into the rock slab at varying locations to produce different pore pressure field. Fractures can be

Fig. 1 Experimental and numerical model setup for Cases Ia–IVa, to study the influence of pore pressure on the tensile fracture propagation



propagated by either the internal hydraulic pressure from one of the injection pores or by the mechanical separation of a notch at the top of the sample. The setup for the numerical simulations and the experimental results is shown in Fig. 1.

Four numerical cases were considered for the first kind of model, and these are labeled with “a”: Case Ia was without pore pressure at the injection holes in a relatively homogeneous rock specimen ($m = 6$), Case IIa included pore pressure at the injection holes in a relatively homogeneous rock specimen ($m = 6$), Case IIIa was without pore pressure at the injection holes in the relatively heterogeneous rock specimen ($m = 3$), and Case IVa included pore pressure at the injection holes in the relatively heterogeneous rock specimen ($m = 3$). Referring to the configuration of the experimental tests (Bruno and Nakagawa 1991), the side length of the square rock slab was 150 mm. The numerical model of the block was the same size, composed of 62,500 (250×250) identical square elements (see Fig. 1). The diameter of each injection hole was 12 mm. The analysis assumed plane strain conditions. The initial coefficient of permeability (k_0) was about 0.04 mDa. The internal constant pore (injection) pressure at Hole 1 was 1.4 MPa, while Hole 2 was maintained at atmospheric conditions. The input material parameters are shown in Table 1. To simulate the experimental tests (Bruno and Nakagawa 1991), the fracture was propagated downward by driving an indenter into a vertical inducing slot at the top of the specimen with displacement control (0.01 mm/step) (see Fig. 1). The strength and elastic modulus of the indenter in the current models were given sufficiently high values such that they did not deform plastically during the rock failure process—see Table 2 (Wang et al. 2011). The

Table 1 Input material mechanical parameters for the first kind of numerical model

Index	Value
Homogeneity index (m)	3, 6
Young’s modulus (E_0)	60,000 MPa
Poisson’s ratio (ν)	0.25
Internal friction angle (ϕ)	30°
Compressive strength (f_c)	60 MPa
Tensile strength (f_t)	6 MPa
Coefficient of residual strength ($f'_{cr}/f'_c = f'_{tr}/f'_t$)	0.1
Permeability (k_0)	0.04 mDa
Internal constant pore pressure at the injection hole (p_c)	1.4 MPa
Coefficient of pore water pressure (α)	0.1
Coupling coefficient (β)	0.05
Mutation coefficient of permeability (ξ)	20

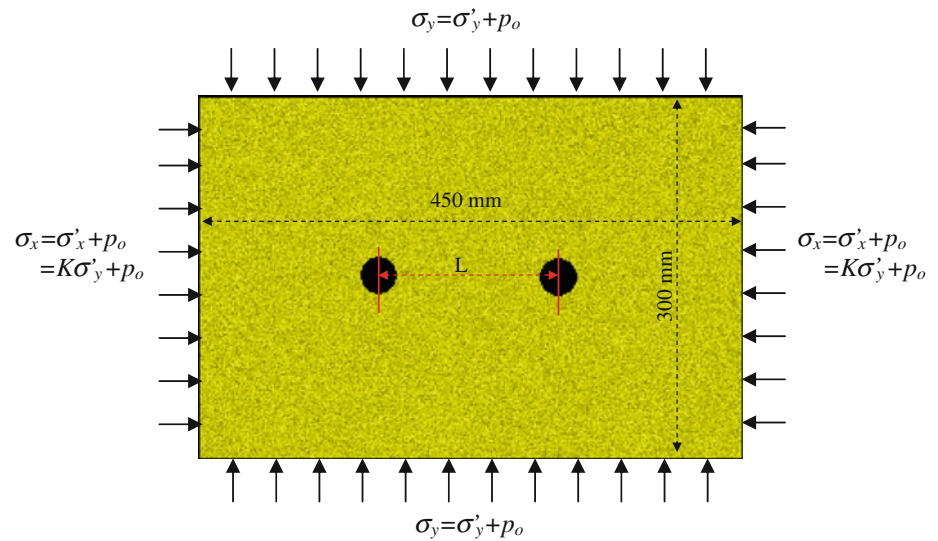
Table 2 Material parameters for the indenter

Elastic modulus	300 GPa
Strength	1,000 MPa
Poisson’s ratio	0.25
Homogeneity index (m)	3

length of the vertical slot was 20 mm. As for the fracture propagated downward by driving an indenter, some researchers used cohesive crack model to investigate this fundamental mechanism (Bolzon et al. 2002; Cocchetti et al. 2002; Saouma et al. 2002). The current work just focuses on the effect of pore pressure on the cracks evolution. The detailed fracturing mechanism of specimens due to the indenter has been discussed by Wang et al. (2011).

Only tensile stress fields were imposed in the laboratory tests of Bruno and Nakagawa (1991) to study the effect of pore pressure magnitude on the tensile fracture evolution. In fact, different in situ stress ratios (K : defined as the initial ratio of σ'_x/σ'_y) could cause both tensile and shear stress fields. Therefore, it is also important to investigate the effect of pore pressure on the evolution fractures in a shear stress field. Furthermore, the effect of the distance between the two injection holes on the fracture propagation between them was not considered in the experimental tests. Therefore, for the second kind of numerical model, another four cases of numerical simulations are reported (see Fig. 2), labeled with “b”. Case Ib was performed to consider the behavior of rock in the vicinity of two holes that were expanding due to increasing external loads and internal constant pore pressure. The purpose was to develop a better understanding of hydraulic fracture initiation, propagation and coalescence mechanisms between two injection holes. For Case IIb, the influence of the heterogeneity on hydraulic fracture propagation was investigated, by adopting values for the homogeneity index, m , of 1.5, 3.0, 5.0 and 8.0, respectively. For Case IIIb, the effect of different in situ stress ratios (K) on hydraulic fracture propagation was studied. The values of K considered were 0.5, 1.0, 1.25, and 1.5, respectively. For Case IVb, the effect of the distance (L) between two injection holes on the fracture initiation and propagation was numerically simulated, by considering L values of 65, 105, 115, and 165 mm, respectively. The input material parameters are shown in Table 3. The two-dimensional plane stress numerical model is shown in Fig. 2. The 450×300 mm domain of analysis was divided into 300×200 (=60,000) elements. The diameter of the two injection holes was 25 mm. The in situ stress ratio K was used to determine the total stresses σ_x and σ_y , that were

Fig. 2 Numerical model setup for Cases Ib–IVb to study the behavior of two horizontal injection holes inside a saturated rock mass. The rock is subjected to different initial in situ stress ratios and an increasing injection pressure. The heterogeneity of the rock, the initial in situ stress ratio (K), the distance between two injection holes and the difference of the pore pressure in the two injection holes can be controlled by the user



then imposed as boundary conditions (see Fig. 2). In order to maintain the difference of pore pressure in the two injection holes, the injection pressure in the each injection hole was then increased in steps of 0.1 MPa, to initiate and propagate cracks around the two injection holes.

It is noted that based on the description of the laboratory test setup by Bruno and Nakagawa (1991), it is not clear whether the sandstone blocks are fully saturated or not. For simplicity, the current code (RFPA) considers just the saturated case and qualitative trends in fracture orientation have been discussed. More quantitative investigations of poroelastic effects on crack propagation will be the subject of future investigations. In addition, this coupled flow, stresses and damage (FSD) model in RFPA2D has been validated in the previous publications (Yang et al. 2001; Tang et al. 2002; Wang et al. 2009).

Table 3 Input material mechanical parameters for the second kind of numerical model

Index	Value
Homogeneity index (m)	1.5, 3, 5, 8
Young's modulus (E_0)	60,000 MPa
Poisson's ratio (ν)	0.25
Internal friction angle (φ)	30°
Compressive strength (f_c)	60 MPa
Tensile strength (f_t)	6 MPa
Coefficient of residual strength ($f'_{cr}/f'_c = f'_{tr}/f'_t$)	0.1
Permeability (k_0)	0.04 mDa
Coefficient of pore water pressure (α)	0.1
Coupling coefficient (β)	0.05
Mutation coefficient of permeability (ξ)	20

4 Numerically Simulated Results and Discussion

4.1 Influence of Pore Pressure Magnitude and Gradient on the Propagation of Tensile Fractures

In this section, the RFPA2D numerical model will be validated by the experimental results (Bruno and Nakagawa 1991). The model setup is shown in Fig. 1.

4.1.1 Numerically Simulated Tensile Fracture Propagation in Relatively Homogeneous Rock for The Case of No Pore Pressure (Case Ia)

In the absence of pore pressure effects (Case Ia), Fig. 3 illustrates the numerically simulated force–penetration curve. Figure 4 shows the numerically simulated process of tensile fracture initiation for steps A–F from Fig. 3. From Fig. 3, the vertical force on the indenter increases in a linear way (A–E), until total tensile failure of the specimen at Stage F. In fact, the indenter provides not only tensile loading onto the crack tip, but also a downward compressive load onto the rock specimen. The stress concentration beneath the indenter can be seen in Fig. 4. As expected, cracking initiates at the end of the vertical inducing slot (Stage A). It is interesting to note that the tensile stress concentrates at the end of crack: since this kind of test configuration is equivalent to a Brazilian disk test, the crack is mainly the tensile crack. When the minor principal stress exceeds the tensile strength of the element at the location of the end of crack (see Eq. 6), the tensile crack propagates. With increasing loading, the force–penetration curve attains its peak value at point E. When the tensile crack approaches the injection holes (Stage D), in fact, the tensile crack changes the stress distribution around the injection holes. The redistribution of the stress between the

Fig. 3 Numerically simulated force–penetration curve for the case of no pore pressure ($m = 6$) (Case Ia)

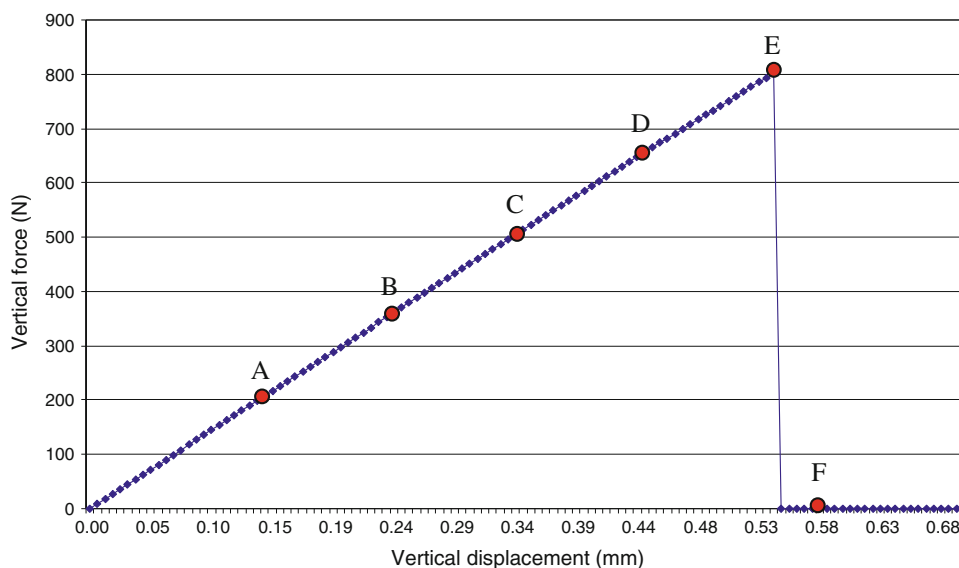
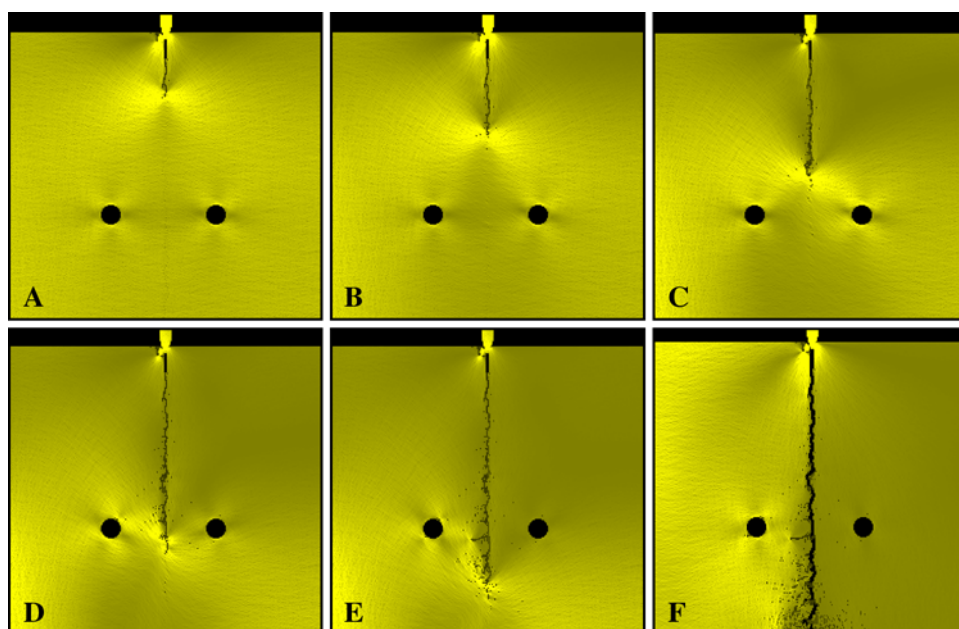


Fig. 4 Numerically simulated tensile fracture propagation in relatively homogeneous rock ($m = 6$) for the case of no pore pressure (yellow and gray shading indicates relative magnitude of the stress field) (Case Ia) (color figure online)



tensile crack and the injection holes can cause the initiation of small fractures from injection holes and the tensile crack.

From Fig. 4d and e, several horizontal fractures propagate from the vertical crack to the left injection hole. It seems that the injection hole has the potential to “attract” the vertical tensile crack to its “field”. Nevertheless, the tensile crack propagates mainly in the vertical maximum compressive stress direction. Finally, in Stage F, the tensile crack separates the specimen into two parts. The comparison of numerical and experimental result is shown in Fig. 5. In both cases, a roughly straight path of tensile fracture is observed. The reason the tensile crack in the experimental test is not the completely vertical (in the

maximum principal stress direction) is probably due to the inherent heterogeneity of the sandstone rock specimen.

Figure 6 shows the effective minimum principal stress distribution along Line 1 (see Fig. 1). From Fig. 6, we can see that the effective minimum principal stress distribution around Hole 1 and Hole 2 (see Fig. 1) are almost the same, which might be expected as the rock specimen is relatively homogeneous. If the material were perfectly homogeneous, the stress distribution around the two injection holes should be completely symmetrical. In addition, in the middle of the two injection holes, the effective minimum principal stress is locally the highest, and it decreases gradually approaching the injection holes along Line 1. This is the reason why the tensile crack propagates through the middle of injection holes.

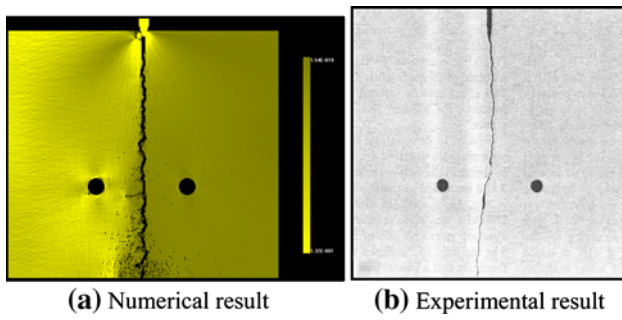
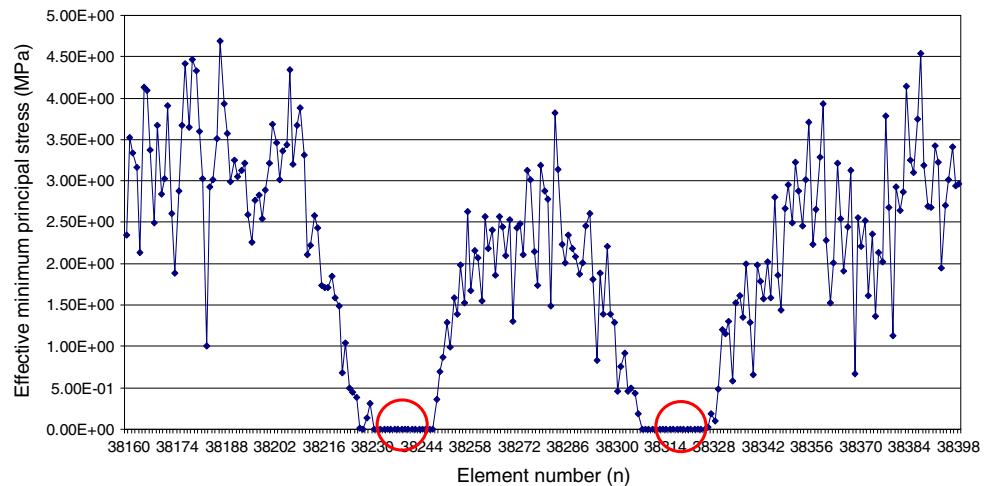


Fig. 5 Comparison of numerical simulation and laboratory test results in relatively homogeneous rock ($m = 6$) for the case of no pore pressure effect (Case Ia: yellow and gray shading indicates relative magnitude of the stress field) (color figure online)

4.1.2 Numerically Simulated Tensile Fracture Propagation in Relatively Homogeneous Rock for the Case of Considering The Effect of Pore Pressure (Case IIa)

Figure 7 illustrates numerically simulated force–penetration curve considering the effect of 1.4 MPa of pore pressure in Hole 1 (Case IIa). From Fig. 7, although the vertical force again increases in a linear way (A–E) until the total tensile failure of the specimen in Stage F, the vertical force is slightly lower than that of Case Ia (see Fig. 3), in which pore pressure effects were absent. For instance, the peak force in Fig. 7 is 721.2 N, while the peak force in Fig. 3 is 801.7 N. This is because the specimen is actually under the combined conditions of vertical stress and internal compressive pore pressure, causing the minimum principal effective stress to be less compressive and more tensile. Accordingly, a smaller vertical force is needed for the failure of specimen. Figure 8 shows the effective minimum principal stress distributions along Line 1 (see Fig. 1) for the Case IIa, and it can be seen that the effective minimum principal stress around Hole 1 is higher than that of Hole 2. Figure 9 shows that pore pressure

Fig. 6 Effective minimum principal stress distributions along Line 1 for the case of no effect of pore pressure (Case Ia)



distribution along Line 1 and across Hole 1 and Hole 2. Because there is no pore pressure in Hole 2, there is certainly no pore pressure distribution around Hole 2. In the vicinity of Hole 1, both the effective minimum principal stress and pore pressure are the highest and they decrease gradually away from the hole.

Figure 10 shows the numerically simulated process of tensile fracture initiation and propagation for Case IIa with Stages A–F, corresponding to Stages A–F in the force–penetration curve for Case Ia in Fig. 7. Figure 10 also shows the pore pressure gradient field (in shades of yellow and gray) during the failure process of the specimen for Case IIa. Initially the pore pressure gradient field is almost concentrically distributed around the center of Hole 1, except for the deviation adjacent to Hole 2. In Stage A, the damaged (failed) elements not only occur at the end of the vertical inducing slot, but also randomly within the pore pressure gradient field. Moreover, with propagation of the tensile crack, the pore pressure gradient field modifies accordingly (see Stages B–F). It indicates that not only the pore pressure magnitude but also the pore pressure gradient can influence the propagation of tensile crack. In addition, when the tensile crack passes through the field between the Hole 1 and Hole 2, a deviation of the crack toward Hole 1 is evident, which is in agreement with the experimental results, as shown in Fig. 11 (Bruno and Nakagawa 1991). In the meantime, some small tensile fractures initiate on the top and bottom of Hole 1 and propagate toward the vertical tensile crack. Such small tensile fractures in Hole 1 would not be easily measured in the laboratory test of Bruno and Nakagawa (1991). The vertical tensile crack does not run into Hole 1, because the vertical maximum principal stress mainly controls the tensile crack direction. Nevertheless, the pore pressure in Hole 1 does affect the path of the tensile crack propagation.

It is noted that, for Cases Ia and IIa, only the relatively homogeneous rock specimens ($m = 6$) were used.

Fig. 7 Numerically simulated force–penetration curve for the case of considering the effect of pore pressure ($m = 6$) (Case IIa)

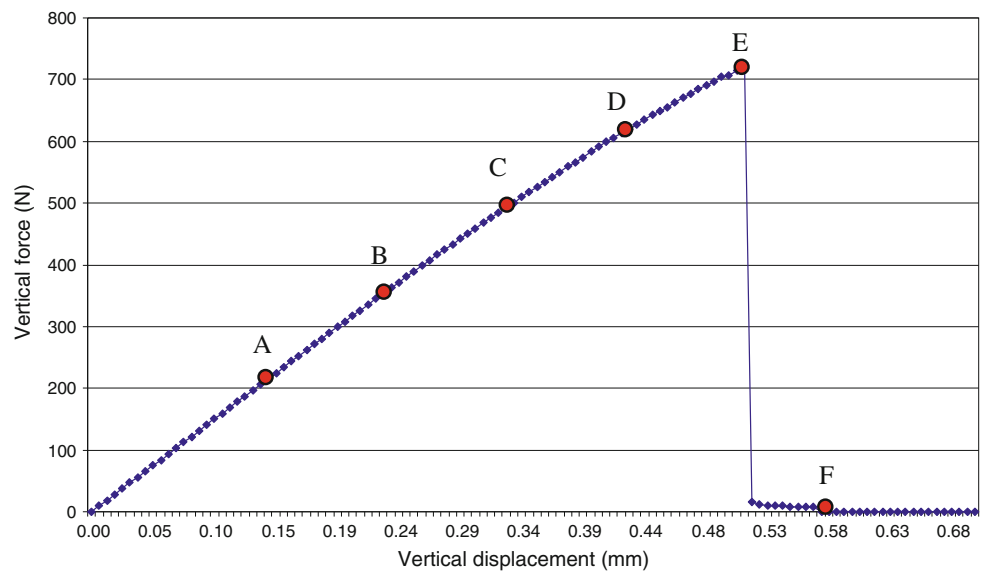


Fig. 8 Effective minimum principal stress distributions along Line 1 for the case of considering the effect of pore pressure (Case IIa)

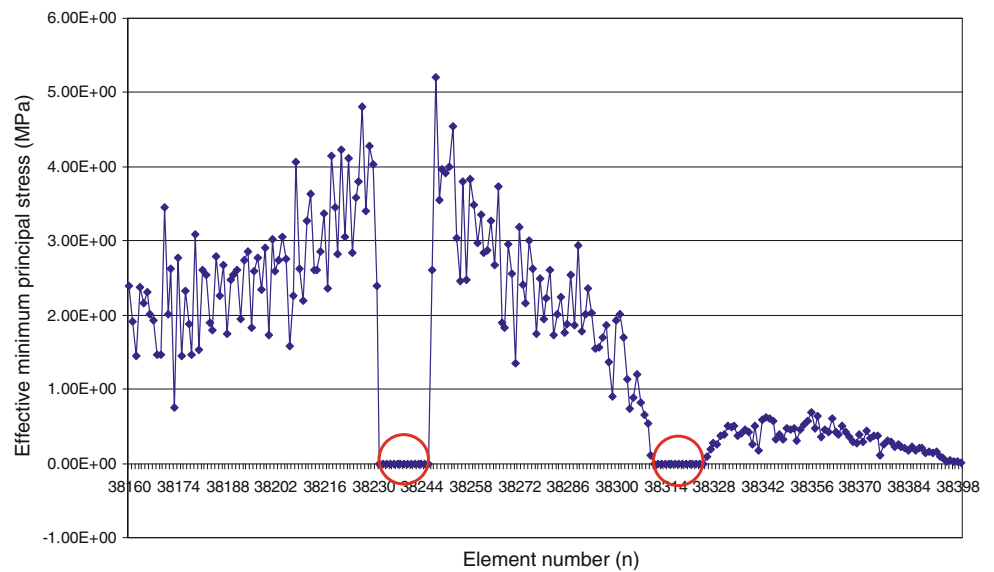


Fig. 9 Pore water pressure distributions along Line 1 for the case of considering the effect of pore pressure (Case IIa)

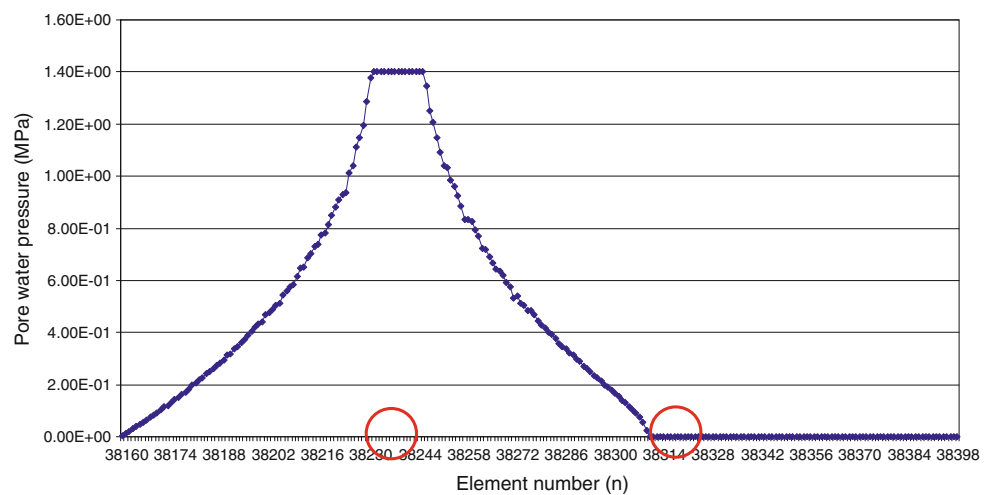


Fig. 10 Numerically simulated tensile fracture propagation in relatively homogeneous rock ($m = 6$) for the case of pore pressure effect (Case IIa: yellow and gray shading indicates relative magnitude of the pore water pressure field) (color figure online)

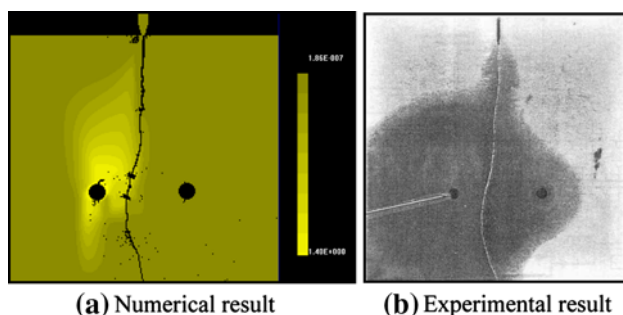
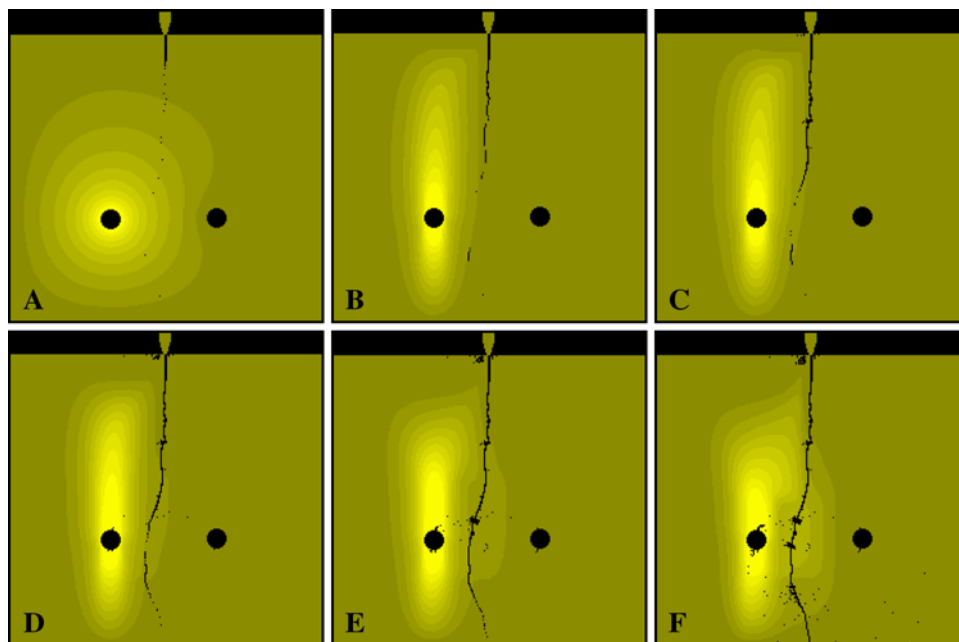


Fig. 11 Comparison of numerical simulation and laboratory test results in relatively homogeneous rock ($m = 6$) for the case of no pore pressure effect (Case IIa: yellow and gray shading indicates relative magnitude of the stress field) (color figure online)

What will happen if the relatively heterogeneous rock specimens ($m = 3$) are adopted in the numerical tests? In Cases IIIa and IVa, the simulations are repeated for relatively heterogeneous ($m = 3$) rock specimens.

4.1.3 Numerically Simulated Tensile Fracture Propagation in Relatively Heterogeneous Rock for the Case of No Pore Pressure (Case IIIa)

Figure 12 illustrates the numerically simulated force–penetration curve for Case IIIa in a relatively homogeneous rock specimen ($m = 3$). Figure 13 shows the stages of tensile fracture initiation and propagation, corresponding with A–F in Fig. 12. Unlike the relatively homogeneous specimen of Case Ia in Fig. 3, due to the greater heterogeneity of the rock specimen, the force–displacement curve is not completely linear before the peak value. Moreover, around the main

tensile crack tip, there are many small fractures in Fig. 13. Particularly when the main tensile crack approaches Hole 1 and Hole 2 (see Stage D), more small cracks initiate from the main tensile crack and propagate to the two injection holes (see Stages D and E). Simultaneously, small tensile fractures initiate from the top and bottom of the injection holes. Eventually, the small cracks from the main tensile crack connect with the cracks originating from Hole 1. At the same time, the main tensile crack continues to propagate downward. Effectively, the propagating fracture divides into two branches, with one running into the Hole 1 and the other one continuing to the bottom of the specimen (see Stage F), which is controlled by the maximum principal stress.

4.1.4 Numerically Simulated Tensile Fracture Propagation in Relatively Homogeneous Rock for the Case of Considering the Effect of Pore Pressure (Case IVa)

Figure 14 illustrates the numerically simulated force–penetration curve for Case IVa in a relatively heterogeneous rock specimen ($m = 3$) considering the effect of 1.4 MPa of pore pressure applied in Hole 1. Figure 15 shows the stages of tensile fracture initiation and propagation, corresponding with A–F in Fig. 14. Figure 14 shows that due to the pore pressure, the force–displacement curve is more nonlinear and the force is lower than that for Case IIIa in Fig. 12. Similar to the results for Case IIa, pore pressure gradient field also changes with the propagation of the main tensile crack. Also similar to the results for Case IIa, the pore pressure causes elements to fail well in advance of the crack tip and many small fractures initiate from the main tensile crack and propagate mainly to

Fig. 12 Numerically simulated force–penetration curve for the case of a relatively heterogeneous rock ($m = 3$) without applied pore pressures (Case IIIa)

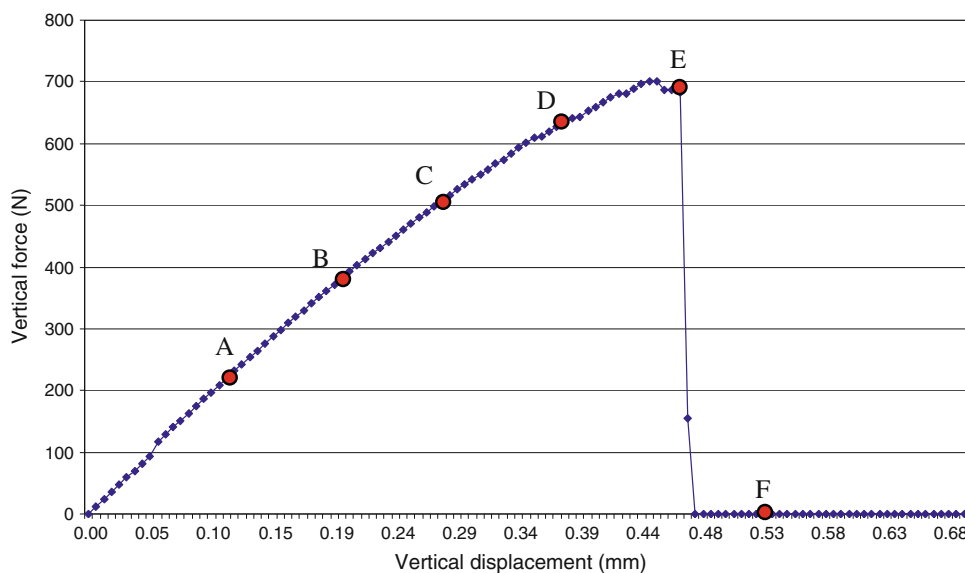
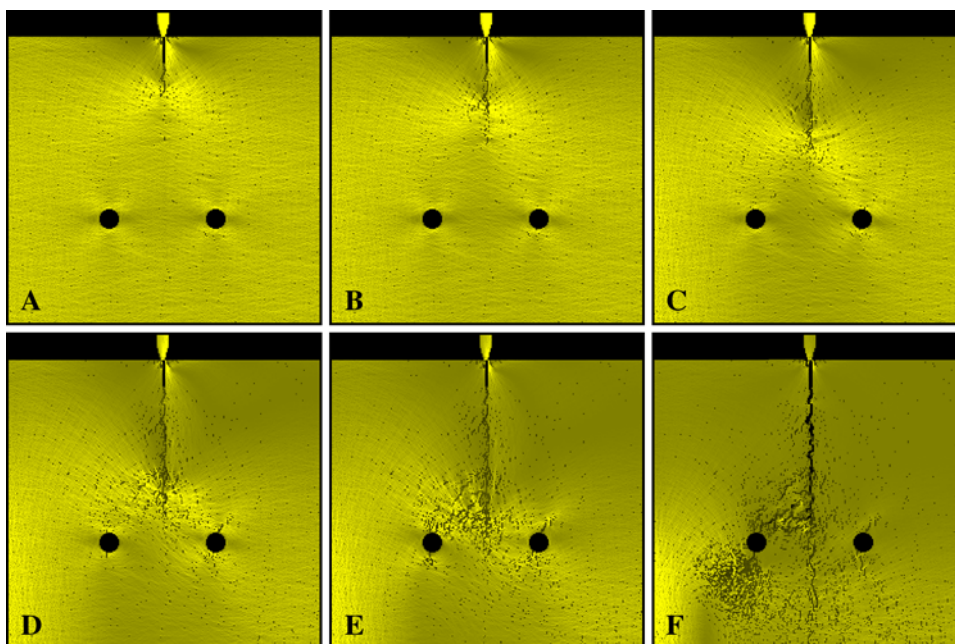


Fig. 13 Numerically simulated tensile fracture propagation in relatively heterogeneous rock ($m = 3$) for the case of no pore pressure effect (Case IIIa: yellow and gray shading indicates relative magnitude of the stress field) (color figure online)



Hole 1. In contrast to Case IIIa, the main tensile crack starts to bend towards Hole 1 from Stage B, and it no longer propagates through the region between the holes. This indicates that the pore pressure gradient field can have a dominating effect on the propagation direction of the main tensile crack.

It is noted that, in RFPA, although the mechanical response of a single mesoscopic element is linear, the macroscopic behavior of a numerical sample (containing a lot of mesoscopic elements) could be nonlinear (Tang et al. 1998). This nonlinear behavior arises from the heterogeneous material properties. The more heterogeneous the material, the stronger the nonlinearity in the stress–strain response. The homogeneity index (m) as used in RFPA2D affects this behavior. For instance, for the case shown in Fig. 7, m is 6, meaning the material is relatively homogeneous and the load–displacement

response is linear. This is in contrast to the case shown in Figs. 12 and 14, where m is 3, meaning the material is relatively heterogeneous and the load–displacement is nonlinear.

4.2 Numerical Modeling of Hydraulic Fracturing of Heterogeneous Rock with Two Injection Holes

4.2.1 Fracture Initiation and Propagation around Two Injection Holes (Case Ib)

Figure 16 shows the numerically simulated hydraulic fracture process with K of 1.0 ($\sigma'_h = 10$ MPa, $\sigma'_v = 10$ MPa). The homogeneity index (m) is 3. The initial injection (pore) pressure is the same (3 MPa) for the two injection holes, and the incremental injection pressure increase (Δp) is 1 MPa for

Fig. 14 Numerically simulated force–penetration curve for a relatively heterogeneous specimen ($m = 3$) with pore pressure applied to Hole 1 (Case IVa)

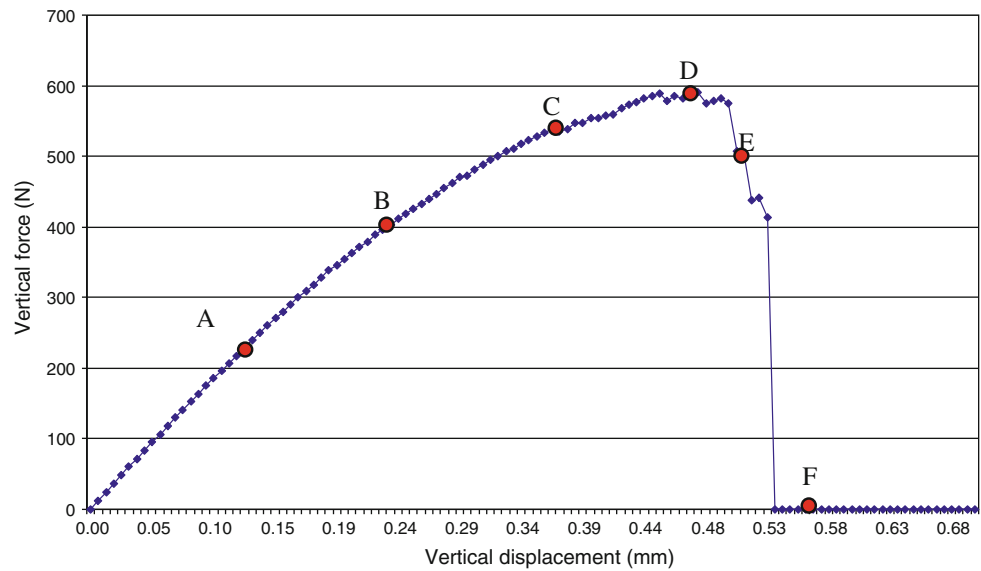
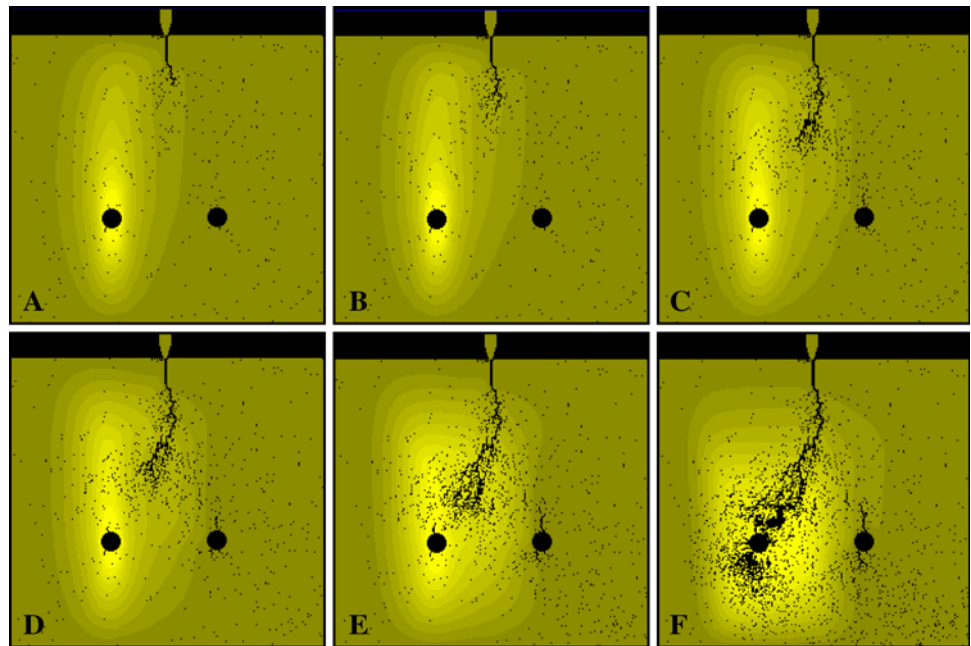


Fig. 15 Numerically simulated tensile fracture propagation in relatively heterogeneous rock ($m = 3$) for the case of pore pressure effect (Case IVa)

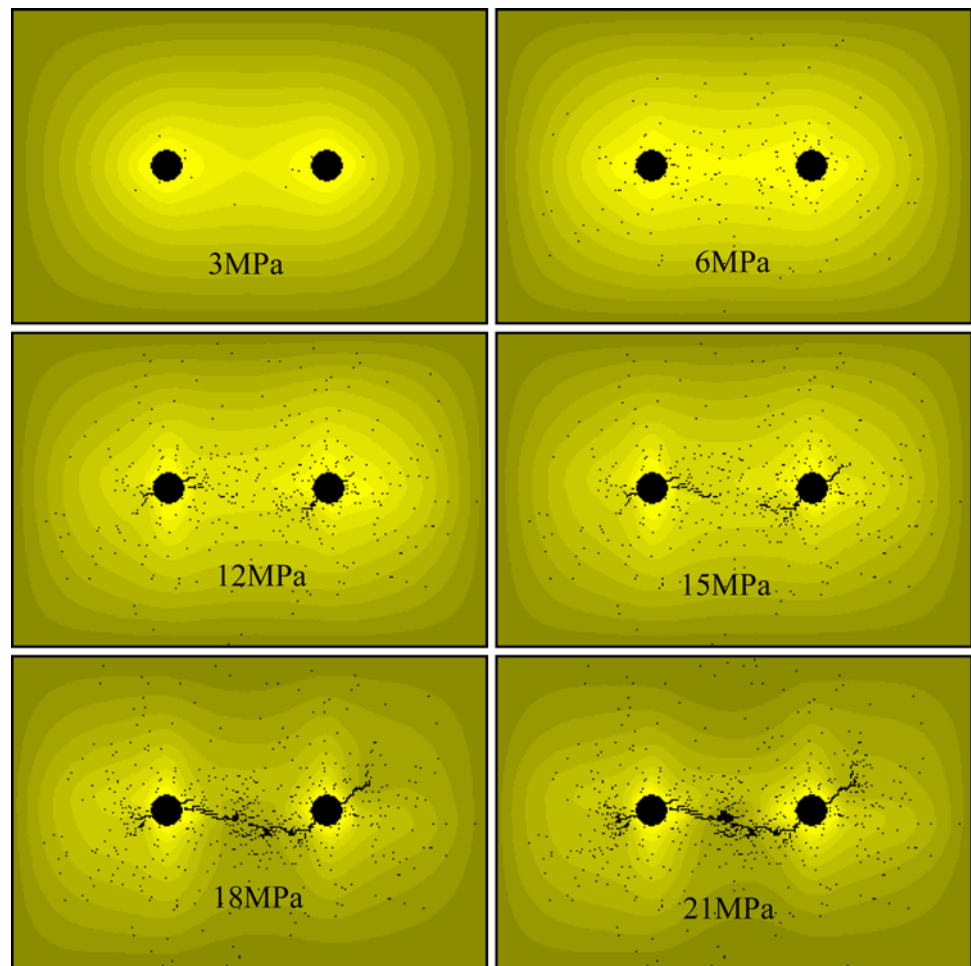


each step. From Fig. 16, with an injection pressure of 3 MPa, there are very few elemental failures around the two injection holes, and no signs of crack initiation. With the increase of injection pressure to about 6 MPa, more and more isolated micro-fractures (damages) start to occur and concentrate on the zone between the two injection holes. Not until the injection pressure reaches 12 MPa, do hydraulic fractures initiate from both injection holes. The propagation of the fracture for the left injection hole (Hole 1) is almost horizontal. In contrast, the propagating direction of the hydraulic fracture from the right injection hole (Hole 2) is about 45° to the horizontal. With an increase of the injection pressure to 15 MPa, both the hydraulic fractures propagate

symmetrically from the two injection holes. However, due to the interaction of the stress field with the two injection holes, hydraulic fractures in the region between the injection holes propagate further than those in regions away from the injection holes. With the injection pressure increased to 18 MPa, the propagation direction of hydraulic fractures from both the right injection hole and left injection holes starts to turn and the fractures tend to coalesce. When the injection pressure is 21 MPa, the two internal hydraulic fractures between the two injection holes have fully coalesced in the horizontal direction, which is the direction of the maximum principal stress.

To investigate the effect of the difference of the pore pressures at the two injection holes on the initiation and propagation

Fig. 16 Numerical simulated failure process of two cavities due to increasing hydraulic pressure, for $K = 1$, $L = 130$ mm, and $m = 3$ (Case Ib: yellow and gray shading indicates relative magnitude of the pore water pressure field) (color figure online)



of hydraulic fractures, three initial conditions are considered. In all cases, the initial pore pressure in Hole 1 is set to 3 MPa, while the initial pore pressure in Hole 2 is set to 4, 5 and 6 MPa, respectively. For each set of initial conditions, the pressure in both holes is increased by an incremental injection pressure (Δp) of 1 MPa, thus the pressures in both holes rise, but the difference in pressure between the holes remains constant. Figure 17 shows that several effects can be observed. Most obviously, with a greater pore pressure difference between Hole 1 and Hole 2, the fractures from the hole with higher pore pressure propagate faster than those from the hole with lower pore pressure. For example, when the pore pressure difference is 1 MPa, the crack length from Hole 1 is much shorter than that from Hole 2. When the pore pressure difference is 2 MPa or 3 MPa, the cracks from Hole 1 are almost inhibited.

4.2.2 Effect of Heterogeneity on Hydraulic Fractures around Two Injection Holes (Case IIb)

In this section, four different values of homogeneity index, $m = 1.5, 3, 5,$ and $8,$ have been chosen to investigate the effect of the heterogeneity of rock on the hydraulic fractures. The results are shown in Fig. 18. For this case, K is

1 and the distance (L) between two injection holes is 130 mm. The boundary conditions and the applied injection pressure are the same as for the case in Sect. 4.2.1.

Figure 18 shows the hydraulic propagation pattern in the four different heterogeneous rock specimen, when the injection pressures are the same with 21 MPa in two injection holes. For a strongly heterogeneous rock material ($m = 1.5$), relative to more homogenous materials ($m = 3, 5$ and 8), more micro-fractures occur, scattered throughout the rock mass, although damage is concentrated in the plane of the two injection holes. Ultimately, two major hydraulic fractures propagate and coalesce in the horizontal direction. As heterogeneity decreases, (the m value increases) under the conditions of an in situ stress field and internal injection pressure, less and less scattered micro-fractures occur around the two injection holes. For a relatively more homogenous material ($m = 8$) almost no isolated micro-fractures are found, with failure/damage restricted to the major hydraulic fractures which initiate, propagate, and coalesce between the injection holes. In summary, due to the heterogeneity of rocks, the hydraulic fracture always selects a path of least resistance through the material with statistical features, which causing the hydraulic fracture paths to be irregular.

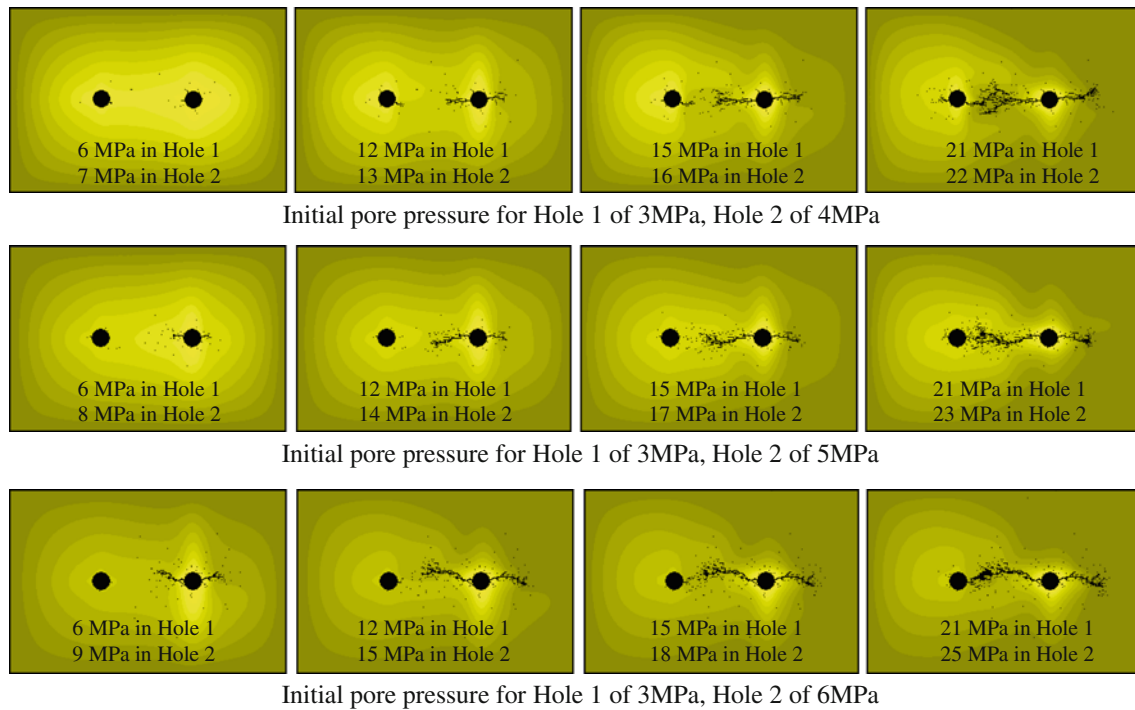
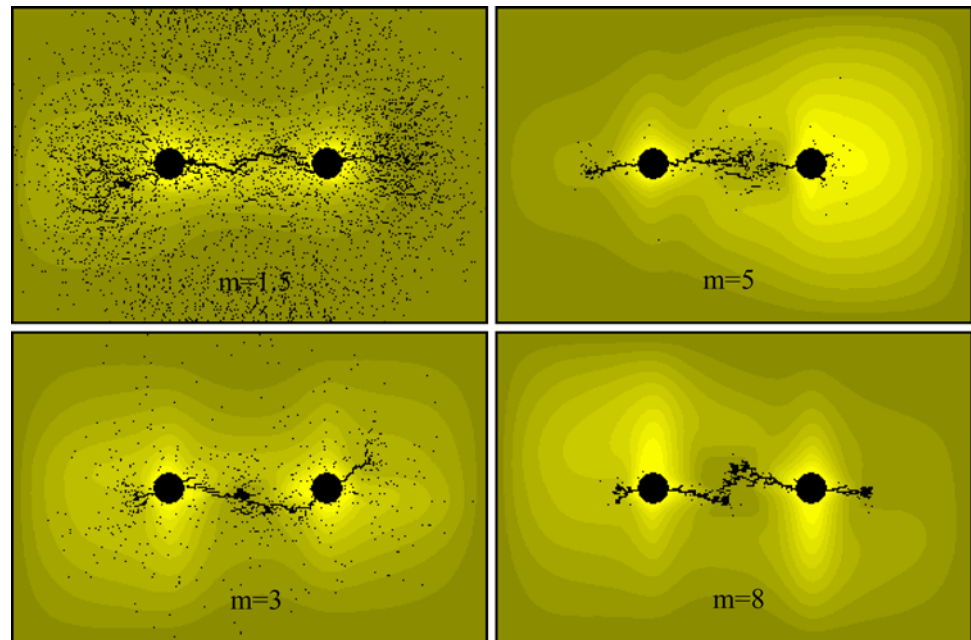


Fig. 17 Numerically simulated failure process of two injection holes due to unequal hydraulic pressures in *left* hole and *right* hole ($K = 1$, $L = 130$ mm, and $m = 3$) (Case Ib: yellow and gray shading indicates relative magnitude of the pore water pressure field) (color figure online)

Fig. 18 Numerically simulated failure patterns of two cavities due to hydraulic pressure with homogeneity index values (m) of 1.5, 3, 5 and 8 ($L = 130$ mm, $K = 1$) (Case Ib: yellow and gray shading indicates relative magnitude of the pore water pressure field) (color figure online)



4.2.3 Effect of Lateral Stress on the Hydraulic Fractures (Case IIIb)

Figure 19 shows the numerically simulated hydraulic fractures for K values of 0.5, 0.75, 1.0, and 1.5, respectively. The homogeneity index (m) for each numerical simulation is

5 (relatively homogenous), and the distance between two injection holes (L) is 130 mm. From Fig. 19, when the horizontal stress is half of the vertical stress (K is 0.5), the directions of hydraulic fractures from both holes are vertical, which is the direction of maximum principal stress for this case. However, due to the small heterogeneity of rock, the

length of two hydraulic fractures is not the same: the left one (Hole 1) is longer than the right one (Hole 2). It is noted that for this case, almost no horizontal hydraulic fractures occur from the injection holes, suggesting that the strongly anisotropic situ stress field dominates the direction of hydraulic fracture, and the effect of one injection hole on the other can be ignored. As a comparison, when K is 0.75, even though K is less than 1, the direction of the hydraulic fracture for Hole 1 is vertical, while the direction of the hydraulic fracture for Hole 2 is horizontal. This result suggests that for this case, hydraulic fracture development is not controlled by the in situ stress field alone, but by both the in situ stress field and the proximity of adjacent injection holes. It also suggests that under this condition, where the influences of stress field and adjacent holes are similar, the direction of crack propagation may ultimately be controlled by the homogeneity of the medium. The effect of the distance between injection holes on the direction of hydraulic fractures is considered further in Sect. 4.2.4.

For the case of $K = 1.0$, as expected, it appears that only the injection pressure and the existence of two injection holes affect the direction of the hydraulic fractures. Although both vertical and horizontal hydraulic fractures occur from the Hole 1, due to the existence of Hole 2, the horizontal hydraulic fractures propagate more strongly than the vertical one, which is poorly developed. For the right hole, there is no vertical hydraulic fracture. When K is 1.5, the direction of maximum principal stress is horizontal and in this case, only horizontal hydraulic fractures from the two injection holes initiate, propagate, and coalesce. Once again, this suggests that in a strongly anisotropic stress field, the stress field dominates the direction of hydraulic

fracture, and the effect of one injection hole on the other can be ignored.

4.2.4 The Influence of the Distance between Two Injection Holes on Hydraulic Fractures (Case IVb)

In this section, four different distances between the two injection holes ($L = 65, 105, 115,$ and 165 mm) have been chosen to investigate the effect of hole spacing on the hydraulic fracture process. For this case, K is 0.75 and m is 5. The initial injection (pore) pressure is the same (3 MPa) for the two injection holes and the incremental injection pressure increase (Δp) in both holes is 1 MPa for each step. The results are shown in Fig. 20, when the injection pressures are the same with 21 MPa in two injection holes.

For the closest spacing of $L = 65$ mm, for, there are three significant hydraulic fractures form around the left injection hole and four significant hydraulic fractures form around the right injection hole. The directions for the hydraulic fractures are neither consistently horizontal nor vertical. It indicates that for the case of two closely spaced injection holes, both the injection pressure and in situ stress field (K) can affect the state of stress between the injection holes, and thus, the initiation and propagation of hydraulic fractures. With the increase of the distance of L , the interaction effect of the two injection holes on hydraulic fractures is decreased, whereas the influence of K is enhanced. For instance, when $L = 105$ mm, near-vertical hydraulic fractures form in both injection holes, although the horizontal hydraulic fractures from the two injection holes coalesce as damage increases. However, when the hole spacing increases to 115 mm, major vertical hydraulic

Fig. 19 Numerically simulated failure process of two cavities due to hydraulic pressure with varying stress ratios: $K = 0.5, 0.75, 1.0, 1.5$ ($L = 130$ mm, $k = 1, m = 5$) (Case IIIb: yellow and gray shading indicates relative magnitude of the pore waterpressure field)

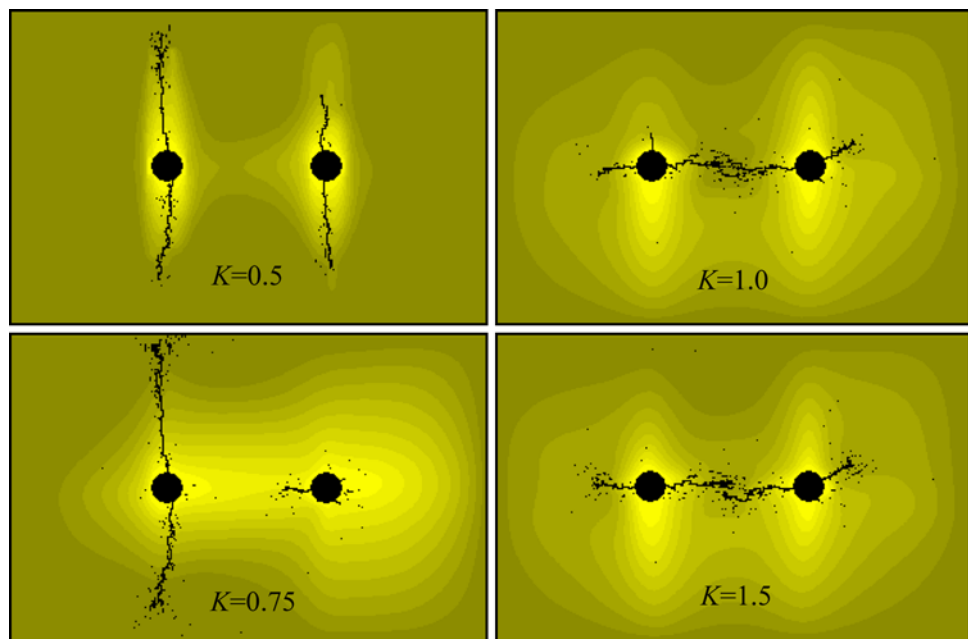
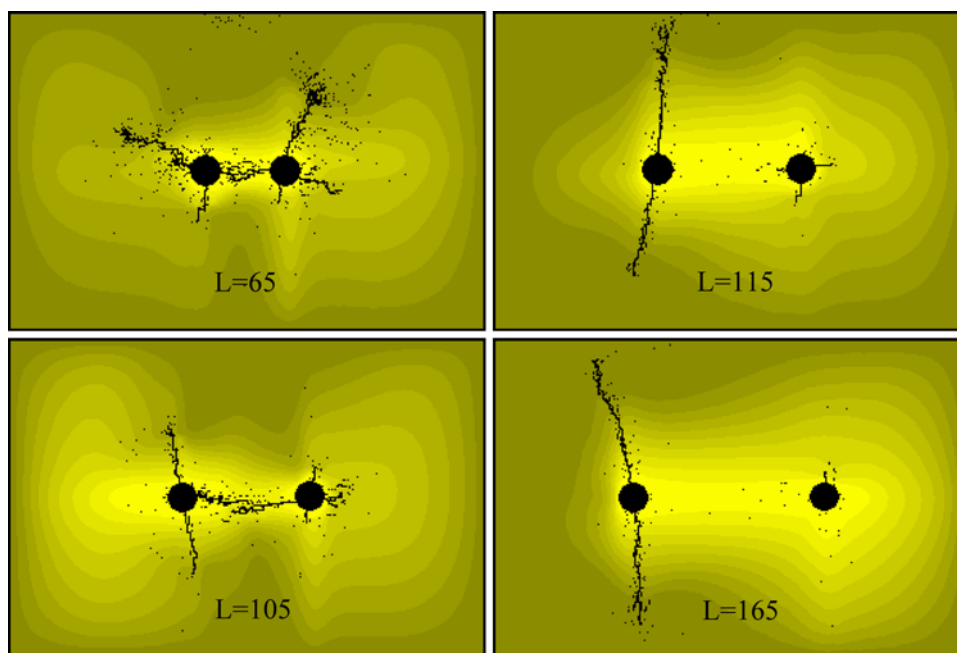


Fig. 20 Numerically simulated failure process of two cavities due to hydraulic pressure with cavity spacings (L) of 65, 105, 115 and 165 mm ($m = 5$, $K = 0.75$) (Case IVb: yellow and gray shading indicates relative magnitude of the pore water pressure field) (color figure online)



fractures form only for the left injection hole, and no horizontal fractures occur. Although the horizontal hydraulic fractures initiate from the right injection hole, they do not propagate to the left. This result indicates that the influence of two injection holes becomes very weak as the spacing increases in excess of five hole diameters. When the spacing reaches 165 mm, no horizontal hydraulic fractures are found during the fracturing process, which indicates that there is no influence from the adjacent holes.

5 Conclusions

In this study, the RFPA2D code was applied to simulate the hydraulic fracturing mechanism in rock. Although the reality is often much more complex than can be simulated by the applied numerical models, the study provides several interesting insights which lead to a better understanding of crack initiation and propagation mechanisms associated with hydraulic fracturing. From the present numerical simulations, the following conclusions are derived.

- In the absence of pore pressure effects, for the relatively homogeneous rock specimen, the roughly straight path of tensile fracture is reproduced by the numerical model, which is in agreement with the experimental results of Bruno and Nakagawa (1991). For the relatively heterogeneous rock specimen, the main tensile fracture was shown to bend towards one of the injection holes.

- When the pore pressure effect is considered, numerically simulated results prove that both the pore pressure magnitude and pore pressure gradient field can influence the tensile fracture propagation, which also agree with the experimental results of Bruno and Nakagawa (1991). In addition, numerical results show that the pore pressure gradient field can be modified with the propagation of tensile crack.
- Generally, in a heterogeneous rock mass, the pressure of fluid injected into parallel horizontal holes will cause localized damage throughout the medium, but concentrated in the vicinity of the holes, and in particular, in the region between the holes. As the injection pressure increases, discrete fractures will initiate and propagate outwards from the holes. If the injection holes are sufficiently close to each other, the propagating cracks will turn and eventually coalesce in the region between the holes.
- The numerical results indicate K is an important parameter in determining the direction of hydraulic fractures in a system with two injection holes. When K is not close to 1.0, and the magnitudes of the principal stresses are significantly different, either vertical or horizontal hydraulic fractures will dominate, in the direction of the maximum principal stress, and independent of the presence of the injection holes. However, when K is close to 1.0, the direction of hydraulic fracturing may be affected by the proximity of one hole to another such that fracturing occurs preferentially in the plane containing the holes, and not in the direction of the major principal stress. Whether

this occurs depends on the particular nature of the in situ stress field and the distance between the injection holes, and to a lesser extent, the homogeneity of the rock mass.

- Rock mass heterogeneity has an important influence on the fracture propagation pattern. As the rock mass becomes more homogenous, damage becomes less dispersed in the region around the two injection holes, and only discrete hydraulic fractures, emanating from the injection holes, are seen to occur.
- The pattern of hydraulic fracturing is dominated by the proximity of adjacent injection holes when they are closely spaced, but their influence decreases as their spacing increases. The influence of an adjacent injection hole becomes negligible at hole spacings greater than about five diameters.

Acknowledgments The work described in this paper was partially supported by ARC Australian Laureate Fellowship Grant FL0992039 and ARC CoE Early Career Award Grant CE110001009, for which the authors are very grateful.

References

- Abou-Sayed AS, Brechtel CE, Clifton RJ (1978) In situ stress determination by hydrofracturing: a fracture mechanics approach. *J Geophys Res* 83(B6):2851–2862
- Berchenko I, Detournay E (1997) Deviation of hydraulic fractures through poroelastic stress changes induced by fluid injection and pumping. *Int J Rock Mech Min Sci* 34(6):1009–1019
- Biot MA (1941) General theory of three-dimensional consolidation. *J Appl Phys* 12(2):155–164
- Bjerrum L, Nash JKTL, Dennard RM, Gibson RE (1972) Hydraulic fracturing in field permeability testing. *Geotechnique* 22(2):319–332
- Bohloli B, de Pater CJ (2006) Experimental study on hydraulic fracturing of soft rocks: influence of fluid rheology and confining stress. *J Petrol Sci Eng* 53(1–2):1–12
- Bolzon G, Fedele R, Maier G (2002) Parameter identification of a cohesive crack model by Kalman filter. *Comput Methods Appl Mech Eng* 191:2847–2871
- Boone TJ, Wawrzynek PA, Ingraffea AR (1986) Simulation of the fracture process in rock with application to hydrofracturing. *In J Rock Mech Min Sci* 23(3):255–265
- Boutt DF, Goodwin L, McPherson BJOL (2009) Role of permeability and storage in the initiation and propagation of natural hydraulic fractures. *Water Resour Res*, 45(W00C13). doi:10.1029/2007WR006557
- Bruno MS, Nakagawa FM (1991) Pore pressure influence on tensile fracture propagation in sedimentary rock. *In J Rock Mech Min Sci* 28(4):261–273
- Cocchetti G, Maier G, Shen XP (2002) Piecewise linear models for interfaces and mixed mode cohesive cracks. *Comput Model Eng Sci* 3(3):279–298
- Crosby DG, Rahman MM, Rahman MK, Rahman SS (2002) Single and multiple transverse fracture initiation from horizontal wells. *J Petrol Sci Eng* 35:191–204
- Detournay E, Atkinson C (2000) Influence of pore pressure on the drilling response in low-permeability shear-dilatant rocks. *In J Rock Mech Min Sci* 37:1091–1101
- Detournay E, Cheng H-DA (1998) Poroelastic response of a borehole in an non-hydrostatic stress field. *Int J Rock mech Min Sci Geomech Abstr* 25(3):171–182
- Detournay E, McLennan JD, Roegiers JC (1986) Poroelastic concepts explain some of the hydraulic fracturing mechanics. SPE Paper 15262 presented at the Unconventional Gas Technol. Symp. of the SPE, Louisville
- Detournay E, Cheng A, Roegiers JC, McLennan JD (1989) Poroelasticity considerations in in situ stress determination by hydraulic fracturing. *In J Rock Mech Min Sci* 26:507–513
- Geertsma J (1985) Some rock-mechanical aspects of oil and gas well completions. *Soc Petrol Engrs J* 25:848–856
- Griffith AA (1920) The phenomena of rupture and flow in solids. *Phil Trans R Soc A221:163–198*
- Guo F, Morgenstern NR, Scott JD (1993) Interpretation of hydraulic fracturing breakdown pressure. *Int J Rock Mech Min Sci Geomech Abstr* 30(6):617–626
- Haimson BC, Fairhurst C (1969) Hydraulic fracturing in porous permeable materials. *J Petrol Technol* 2(1):811–817
- Hossain MM, Rahman MK, Rahman SS (2000) Hydraulic fracture initiation and propagation: roles of wellbore trajectory, perforation and stress regimes. *J Pet Sci Eng* 27:129–149
- Hubbert MK, Willis DG (1957) Mechanics of hydraulic fracturing. *Trans AIME* 210:153–163
- Jaeger JC (1963) Extension failure in rocks subjected to fluid pressure. *J Geophys Res* 68:1759–1765
- Jaeger JC, Cook NG (1979) Fundamentals of rock mechanics, 3rd edn. Chapman & Hall, London
- Krajcinovic D (1996) *Damage Mechanics*. Elsevier, Amsterdam
- Lo KY, Kaniaru K (1990) Hydraulic fracture in earth and rock fill dams. *Can Geotech J* 27(4):496–506
- Medlin WL, Masse L (1979) Laboratory investigation of fracture initiation pressure and orientation. *Soc Petrol Engrs J* 19:129–144
- Noghabai K (1999) Discrete versus smeared versus element-embedded crack models on ring problem. *J Eng mech* 125(3):307–315
- Rubin MR (1983) Experimental study of hydraulic fracturing in an impermeable material. *J Energy Resour Technol* 105:116–124
- Rummel F (1987) Fracture mechanics approach to hydraulic fracturing stress measurements. *In: Atkinson B (ed) Fracture mechanics of rock*, Academic Press, New York, p 317–239
- Saouma V, Natekar D, Sbaizero O (2002) Nonlinear finite element analysis and size effect study of a metal-reinforced ceramics-composite. *Mater Sci Eng A323:129–137*
- Tang CA (1997) Numerical simulation on progressive failure leading to collapse and associated seismicity. *Int J Rock Mech Min Sci* 34:249–262
- Tang CA, Yang WT, Fu YF, Xu XH (1998) New approach to numerical method of modelling geological processes and rock engineering problems—continuum to discontinuum and linearity to nonlinearity. *Eng Geol* 49(3–4):207–214
- Tang CA, Tham LG, Lee PKK, Yang TH, Li LC (2002) Coupled analysis of flow, stress and damage (FSD) in rock failure. *Int J Rock Mech Min Sci* 39(4):477–489
- Thallak S, Rothenbury L, Dusseault M (1991) Simulation of multiple hydraulic fractures in a discrete element system. *In: Roegiers JC (ed) Rock mechanics as a multidisciplinary science*, Proceedings of the 32nd US Symposium. Balkema, Rotterdam, pp 271–280
- Wang MS, Nakagawa FM (1991) Pore pressure influence on tensile fracture propagation in sedimentary rock. *Int J Rock Mech Min Sci* 28(4):261–273
- Wang SY, Sun L, Au ASK, Yang TH, Tang CA (2009) 2D-numerical analysis of hydraulic fracturing in heterogeneous geo-materials. *Constr Build Mater* 23:2196–2206
- Wang SY, Sloan SW, Liu HY, Tang CA (2011) Numerical simulation of the rock fragmentation process induced by two drill bits

- subjected to static and dynamic (impact) loading. *Rock Mech Rock Eng* 44:317–336
- Warpinski NR, Teufel LW (1987) Influence of geologic discontinuities on hydraulic fracture propagation. *J Petrol Technol* 39(2): 209–220
- Weibull W (1951) A statistical distribution function of wide applicability. *J Appl Mech* 18:293–297
- Yanagisawa E, Panah AK (1994) Two dimensional study of hydraulic fracturing criteria in cohesive soil. *Soils Found* 34(1):1–9
- Yang TH, Tang CA, Zhu WC, Feng QY (2001) Coupling analysis of seepage and stress in rock failure process. *Chinese J Rock Soil Eng* 23(4):489–493
- Zhu WC, Tang CA (2004) Micromechanical model for simulating the fracture process of rock. *Rock Mech Rock Eng* 37:25–56